IEICE TRANS. ELECTRON., VOL.E107–C, NO.6 JUNE 2024

INVITED PAPER *Special Section on Current Situation of Ultra-High Sensitivity Magnetic Sensors and Measurement Techniques: Present Location of SQUID Sensors*

Simulation of Scalar-Mode Optically Pumped Magnetometers to Search Optimal Operating Conditions

Yosuke ITO[†a)], **Tatsuya GOTO**[††], ***and*** **Takuma HORI**[††], ***Nonmembers***

SUMMARY In recent years, measuring biomagnetic fields in the Earth's field by differential measurements of scalar-mode OPMs have been actively attempted. In this study, the sensitivity of the scalar-mode OPMs under the geomagnetic environment in the laboratory was studied by numerical simulation. Although the noise level of the scalar-mode OPM in the laboratory environment was calculated to be 104 pT/$\sqrt{\text{Hz}}$, the noise levels using the first-order and the second-order differential configurations were found to be 529 fT/cm/$\sqrt{\text{Hz}}$ and 17.2 fT/cm^2/$\sqrt{\text{Hz}}$, respectively. This result indicated that scalar-mode OPMs can measure very weak magnetic fields such as MEG without high-performance magnetic shield roomns. We also studied the operating conditions by varying repetition frequency and temperature. We found that scalar-mode OPMs have an upper limit of repetition frequency and temperature, and that the repetition frequency should be set below 4 kHz and the temperature should be set below 120 °C.

key words: *optically pumped magnetometer (OPM), scalar-mode OPM, differential measurement*

1. Introduction

Magnetic fields caused by neural activities in human brains are extremely weak, less than hundreds of femtotesla, although the brain magnetic fields contain information on neural activities and is expected to be useful for medical applications and elucidation of brain function. In addition, due to the consistent permeability of the human body across different anatomical regions, magnetoencephalography (MEG) offers the advantage of higher precision in the signal source estimation compared to electroencephalography (EEG).

For measurements of such extremely-weak magnetic fields, superconducting quantum interference devices (SQUIDs), which are state-of-the-art and well-developed sensors, have been conventionally used. SQUIDs are high-sensitivity magnetic sensors whose sensitivity is several fT/$\sqrt{\text{Hz}}$ [1]. However, they require cryogenic cooling with liquid helium, resulting in high running costs. In addition, against the backdrop of the current helium price escalation and its increasing scarcity, there is a demand for ultra-high sensitivity magnetic sensors that operate without the requirement of liquid helium.

Manuscript received July 24, 2023.
Manuscript revised October 12, 2023.
Manuscript publicized December 4, 2023.

[†]The author is with the Department of Electronical Engineering, Graduate School of Engineering, Kyoto University, Kyoto-shi, 615–8510 Japan.
[††]The authors were with the Department of Electronical Engineering, Graduate School of Engineering, Kyoto University, Kyoto-shi, 615–8510 Japan.
a) E-mail: yito@kuee.kyoto-u.ac.jp
DOI: 10.1587/transele.2023SEI0002

Optically pumped magnetometers (OPMs) are sensors that detect magnetic fields by observing the spin polarization dynamics in alkali metal atoms. OPMs exhibit extremely high sensitivity and do not necessitate the use of liquid helium. Consequently, they have gained significant attention as magnetic sensors for biomagnetic-field measurements. Theoretical limitation of the sensitivity of OPMs is in the range of tens aT/$\sqrt{\text{Hz}}$ under Spin-exchange relaxation free (SERF) conditions where the relaxation due to spin exchange collisions is negligible [2], [3]. In order to measure magnetic fields under SERF conditions, a magnetic shield room is required to suppress the ambient magnetic field including the Earth's field less than several tens nT. However, installing such high-performance magnetic shield rooms requires an expensive initial investment, which is an obstacle to the introduction of biomagnetic-field measurements.

To solve this problem, many attempts have been made in recent years to realize biomagetic-field measurements in Earth's ambient fields [4], [5]. Limes *et al.* demonstrated biomagnetic-field measurements without any magnetic shields with scalar-mode OPM and differential configuration and the noise level of 16 fT/cm/$\sqrt{\text{Hz}}$ [4]. In this study, we theoretically investigated the sensitivity under the laboratory environment by numerical simulation. In addition, we varied the repetition frequency and temperature, and calculated the change in sensitivity to determined the operating conditions of scalar-mode OPMs.

2. Principle

The principle of the scalar-mode OPMs is shown in Fig. 1 [6]. First, circularly-polarized pump beam whose wavelength is tuned to resonant wavelength of the alkali-metal atoms is emitted to alkali-metal atoms parallel to the bias magnetic field. It causes spin polarization. Then, RF pulses are irradiated to flip the spin polarization. The spin polarization precesses around the bias field and flip back to the direction parallel to the bias field. The free precession frequency is measured by the change of the polarization plane of the linearly-polarized probe beam. When the magnetic field to be measured B_{m} is applied parallel to the bias field, $B = B_0 + B_{\text{m}}$ is calculated from Eq. (1) and the free precession frequency f_{FID}:

$$B = \frac{2\pi f_{\text{FID}} q}{\gamma_e}, \tag{1}$$

where q is the slow-down factor and γ_e is the gyromagnetic

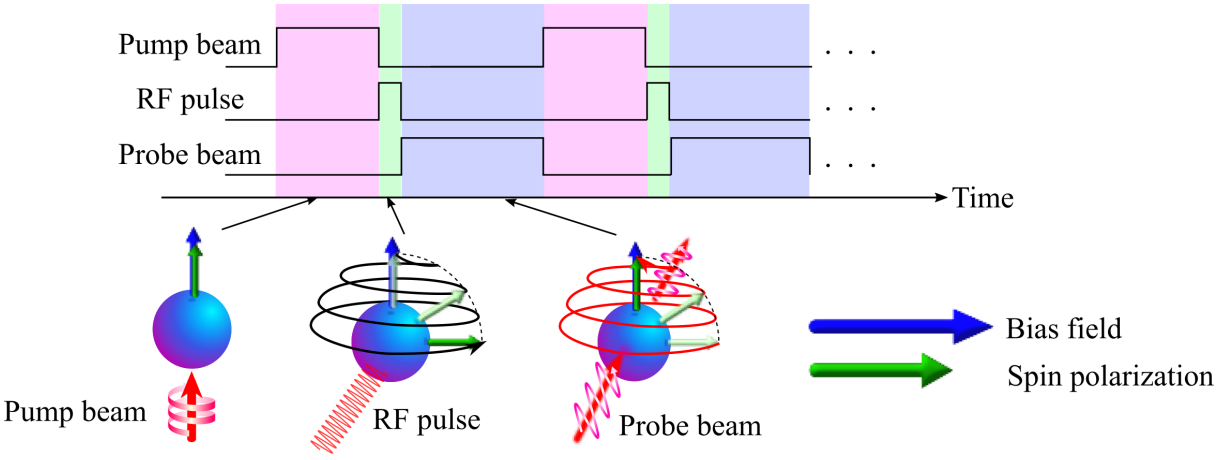

Fig. 1 Sequence of scalar-mode OPMs. In the pumping section, the spin polarization is generated. The spin polarization is flipped by the RF pulse in the RF pulse section, and the free precession frequency during free induction decay is measured in probe section.

ratio of the isolated electron ($|\gamma_e| \sim 1.76 \times 10^{11}$ rad/(s T)). The above process is repeated to measure the time evolution of the magnetic field. Sheng *et al.* used two pulses of the probe beam in one cycle of the measurement scheme, leading to suppressing the spin relaxation caused by the probe beam because it does not occur when the probe beam is off [6]. On the other hand, by continuously irradiating the probe beam, it is possible to simplify the measurement system; therefore, this approach was employed in this study.

In the procedure described above, the spin polarization of the alkali-metal atoms follows the Bloch equation [7].

$$\frac{d}{dt}\boldsymbol{S} = D\nabla^2\boldsymbol{S} + \frac{\gamma_e}{q}\boldsymbol{S}\times\boldsymbol{B} - \frac{R_2}{q}\boldsymbol{S} + \frac{1}{2q}R_{\mathrm{OP}}\boldsymbol{e}_z\,, \tag{2}$$

where D is the diffusion constant of the alkali-metal atom, $\boldsymbol{S}$ is the spin polarization of the electron, $\boldsymbol{B}$ is the magnetic field vector, R_2 is the spin relaxation rate, R_{OP} is the optical pumping rate, and $\boldsymbol{e}_z$ is the unit vector in the z direction. Also, q is expressed using the magnitude of spin polarizastion S as follows [8]:

$$q = \frac{6 + (2S)^2}{1 + (2S)^4}\,. \tag{3}$$

In the case of ^{39}K, q takes values between 4 and 6.

3. Method

We carried out numerical simulation with Bloch equation and rate equations [9], [10].

The simulation geometry is shown in Fig. 2. The alkali-metal atoms were enclosed in the sensor cell whose size was $50\times50\times50$ mm^3 to carry out differential measurement in the cell. We considered the case where the pump beam with a diameter of 8 mm is irradiated in the z direction into the cell. For differential measurements, we introduced three probe beams in x direction. Each probe beam is irradiated with a diameter of 1 mm. The diameter of the pump and probe

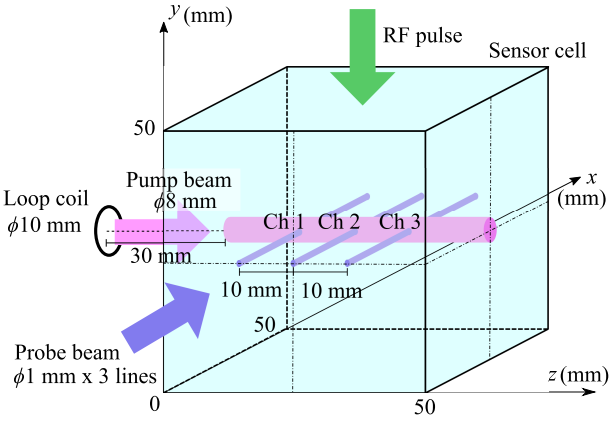

Fig. 2 Simulation model of scalar-mode OPM. The pump beam was irradiated from z direction, and probe beams were irradiated from x direction. RF pulse was irradiated from y direction.

beams were determined for practical application. When the diameter is too small, it leads to a reduction in the number of atoms relevant to the measurement, resulting in a weaker signal. Conversely, when it is too large, it becomes sensitive to the influence of magnetic field gradients, making accurate measurements unfeasible. The distance between the each probe beam was set to 10 mm. The voxel size was set to 1 mm per side, the sensor cell was divided into $51 \times 51 \times 51$, and numerical calculations were performed at each lattice point.

Helium and nitrogen at a ratio of 10:1 and total pressure of 90 kPa at 300 K were enclosed with potassium in the sensor cell as buffer and quenching gases. The gas mixture ratio was set to the value of our group's previous study [13] and the total gas pressure was determined based on the Ref [4]. Potassium was vaporized by heating the sensor cell. We assumed that the temperature in the sensor cell was uniform. The saturated atom density of potassium was expressed as a function of cell temperature T as follows [11]:

$$n_{\mathrm{K}}^{0} = \frac{10^{26.268-4453/T}}{T}. \tag{4}$$

The density of potassium in the cell was assumed to be half of the saturated density because it is reduced below the saturation vapor pressure density due to the presence of trace impurities and the effects of long-term degradation. The pump beam was set to an intensity of 1 W and a wavelength of 770.11 nm, which is the resonant wavelength of potassium. The probe beam was set to an intensity of 5 μW and a wavelength of 770.05 nm, which is slightly detuned from the resonant wavelength. When the probe light is tuned to the resonant wavelength of potassium, it is absorbed by potassium atoms, leading to a disturbance in the spin polarization. Conversely, if it deviates too much from the resonant wavelength, it cannot detect spin polarization state. Hence, it is essential to maintain a slight detuning from the resonant wavelength. This detuning range is determined by factors such as gas pressure and laser light intensities, and in this instance, 770.05 nm was found to optimize the signal.

We assessed the strength of the Earth's field and ambient magnetic field noise in our laboratory in Kyoto with a fluxgate sensor and found that the Earth's field and ambient field noise were 39.2 μT and 99.8 pT/$\sqrt{\mathrm{Hz}}$, respectively. Therefore, we adopted these values for the simulation. The direction of the Earth's field was set to the z axis as a bias field. Furthermore, assuming that the alternating current components of environmental magnetism are generated by seven measurement devices located in the laboratory, noise sources were placed at the following seven coordinates: (x, y, z)=(4 m, 0 m, 0 m), (0 m, 0 m, 4 m), (0 m, 0 m, −4 m), (−9 m, 0 m, 0 m), (0 m, 0 m, 10 m), (−2.6 m, −0.5 m, −0.5 m), (−2.6 m, −0.5 m, −0.5 m), (2.1 m, −0.9 m, 0 m), and (2.1 m, −0.9 m, 0 m), and white Gaussian noise was applied form those sources. In addition, measured utility power supply noise of 60 Hz and 8.82 nT was also applied from above noise sources. The frequency of the RF pulse f_{RF} was set to be Larmor frequency of the bias field B_0. The duty ratio of the pump beam pulse was set to 0.5, and the RF pulse was set to 40 μs.

The test magnetic field of 40 Hz was applied from a loop coil. The strength calculated by Biot-Savart's Law was 50 pT, 30.4 pT, and 19.8 pT in Ch. 1, Ch. 2, and Ch. 3, respectively. Under these conditions, Eq. (2) was calculated numerically using the fourth-order Runge-Kutta method with the time step of 0.25 μs to obtain the time evolution of the spin polarization. For the simplicity, we ignored the diffusion term, because the diffusion length was sufficient smaller than the distance between channels [12].

From the time evolution of the x component of the spin polarization, we calculated the time variation of the OPM output using a conversion efficiency of a photodiode of a polarimeter 0.5 A/W and a current-to-voltage conversion factor of an amplifier 1.0×10^4. f_{FID} was calculated from the number of points that intersected zero in one repetitive measurement section, and the magnetic field detected at each channel was calculated using Eq. (1). Finally, the difference between the obtained magnetic field at each channel was taken as the differential output. The output $B_{1\mathrm{st}}$ was calcualted by following equation:

$$B_{1\mathrm{st}} = \frac{B_1 - B_2}{d}, \tag{5}$$

where B_1 and B_2 were obtained magnetic fields at Ch. 1 and Ch. 2, respectively. d was distance between channels. The output $B_{2\mathrm{nd}}$ was calculated by following equation:

$$B_{2\mathrm{nd}} = \frac{(B_1 - B_2) - (B_2 - B_3)}{d^2}, \tag{6}$$

where B_3 was obtained magnetic fields at Ch. 3.

From the Eqs. (5) and (6), the theoretical values of $B_{1\mathrm{st}}$ and $B_{2\mathrm{nd}}$ were calculated as 19.6 pT/cm and 9 pT/cm^2. When compared to the magnetic field value in Ch. 1, $B_{1\mathrm{st}}$ and $B_{2\mathrm{nd}}$ had magnitudes of 39.2% and 18%, respectively. We varied repetition frequency and temperature, and calculated the signal-to-noise ratio (SNR) in each condition.

4. Results and Discussion

The time variation of each directional component of spin polarization and the output in Ch. 1 is shown in Fig. 3. The repetition frequency and temperature were 2 kHz and 110°C. Figure 3 (a) shows that the spin polarization is generated in z direction during the pumping section, and the spin polarization is knocked down in the xy plane during the RF pulse. From Fig. 3 (b), it can be confirmed that the output has the same time variation as the x direction component of the spin polarization in Fig. 3 (a). From the result of the numerical calculation, the oscillation frequency was about 224 kHz, which was consistent with the value calculated by Eq. (1) with the slow-down factor $q \sim 4.9$. The frequency shift caused by the test fields was several hundreds mHz even in Ch. 1. It is beyond the frequency resolusion of Fourier transform. Therefore, we counted zero-crossing points in FID sections to calculate magnetic fields detected with the OPMs.

The magnetic field calculated by the free precession frequency obtained from the OPM output for each channel is shown in Fig. 4 (a). Each plot approximately overlaps with one another because the 60-Hz power supply field of 8.82 nT and ambient noise were dominant. From the inlet, we could observe slight difference among data points at each channel. The frequecy spectrum of obtained magnetic field in Ch. 1 was shown in Fig. 4 (b), and the noise level was 104 pT/$\sqrt{\mathrm{Hz}}$. This value was similar to the ambient field noise and greater than the 40-Hz applied magnetic field of 50 pT.

Next, the differential output of obtained magnetic fields between Ch. 1 and Ch. 2 was shown in Fig. 5 (a). Obvious 60-Hz noise was diminished. Figure 5 (b) shows frequency spectrum of Fig. 5 (a). The test signal of 40-Hz can be observed, although the 60-Hz peak was still large. The magnitude of 40-Hz test signal was 17.9 pT/cm, and it exhibited an error of approximately 8.7% in comparison to the theoretical value. The noise level was 529 fT/cm/$\sqrt{\mathrm{Hz}}$. This value

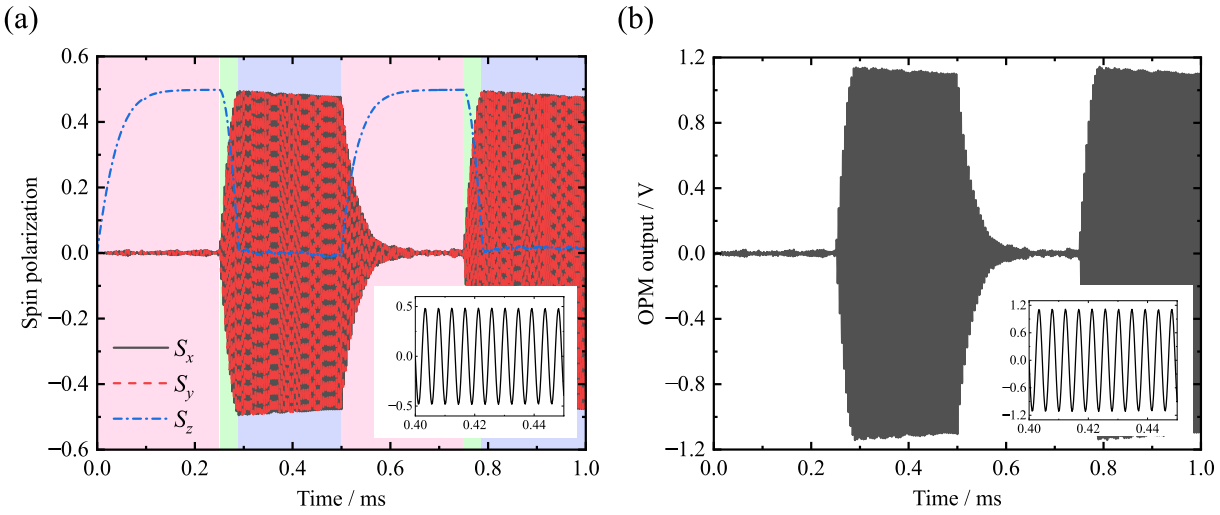

Fig. 3 (a) Time evolution of spin polarization and (b) OPM output obtained from probe beam in Ch. 1. Repetition frequency is 2 kHz, and temperature is 110 °C. The inlets show enlarged graphs of time evolution of S_x (a) and OPM output (b).

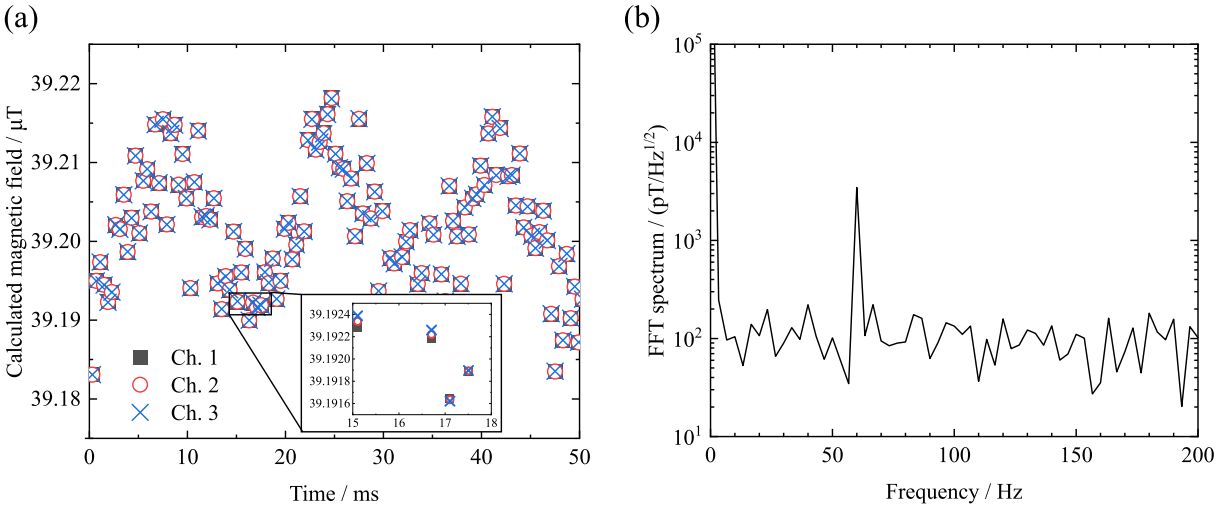

Fig. 4 (a) Calculated magnetic field of each channel. The inlet shows enlarged graph. The free precession frequency obtained from each channel was converted to magnetic fields by Eq. (1). One point in the graph was calculated with one cycle of (b) Frequency spectrum of calculated magnetic field of Ch.1.

was worse than the previous report [4], but it was due to the ambient magnetic field condition. Figure 5 (c) shows differential output among Ch. 1, Ch. 2, and Ch. 3. The 40-Hz test signal was clearly observed and the strength was 7.8 pT/cm^2, which had an error of about 13% compared to the theoretical value. Figure 5 (d) is the frequency spectrum of Fig. 5 (c). The noise level was 17.2 fT/cm^2/$\sqrt{\text{Hz}}$.

The numerical calculation of the change in SNR when the repetition frequency and temperature were varied was shown in Fig. 6. This shows that SNR of about 180 and a noise level of about 20 fT/cm^2/$\sqrt{\text{Hz}}$ were achieved at a small repetition frequency. However, the SNR decreased as the repetition frequency and temperature were increased.

In the simulation, focusing on the noise level of the obtained magnetic field at Ch. 1, it was almost the same as the magnitude of the environmental magnetic noise. However, the noise level was reduced to 529 fT/cm/$\sqrt{\text{Hz}}$ by the differential output of Ch. 1 and Ch. 2, and 17.2 fT/cm^2/$\sqrt{\text{Hz}}$ under the 2nd-order differential output among Ch. 1, Ch. 2, and Ch. 3.

We considered better operating conditions of scalar-mode OPMs. First, we discussed that the SNR decreased as the repetition frequency was increased. The time evolution of spin polarization when the repetition rate was 6 kHz was shown in Fig. 7. In the case, the SNR of 2nd-order differential measurements was about 11, which was worse condition from Fig. 6. The x and y components of the spin polarization did not disappear completely and remained until just before the RF pulse were applied. Due to this effect, the magnitude of the spin polarization in the FID section was different

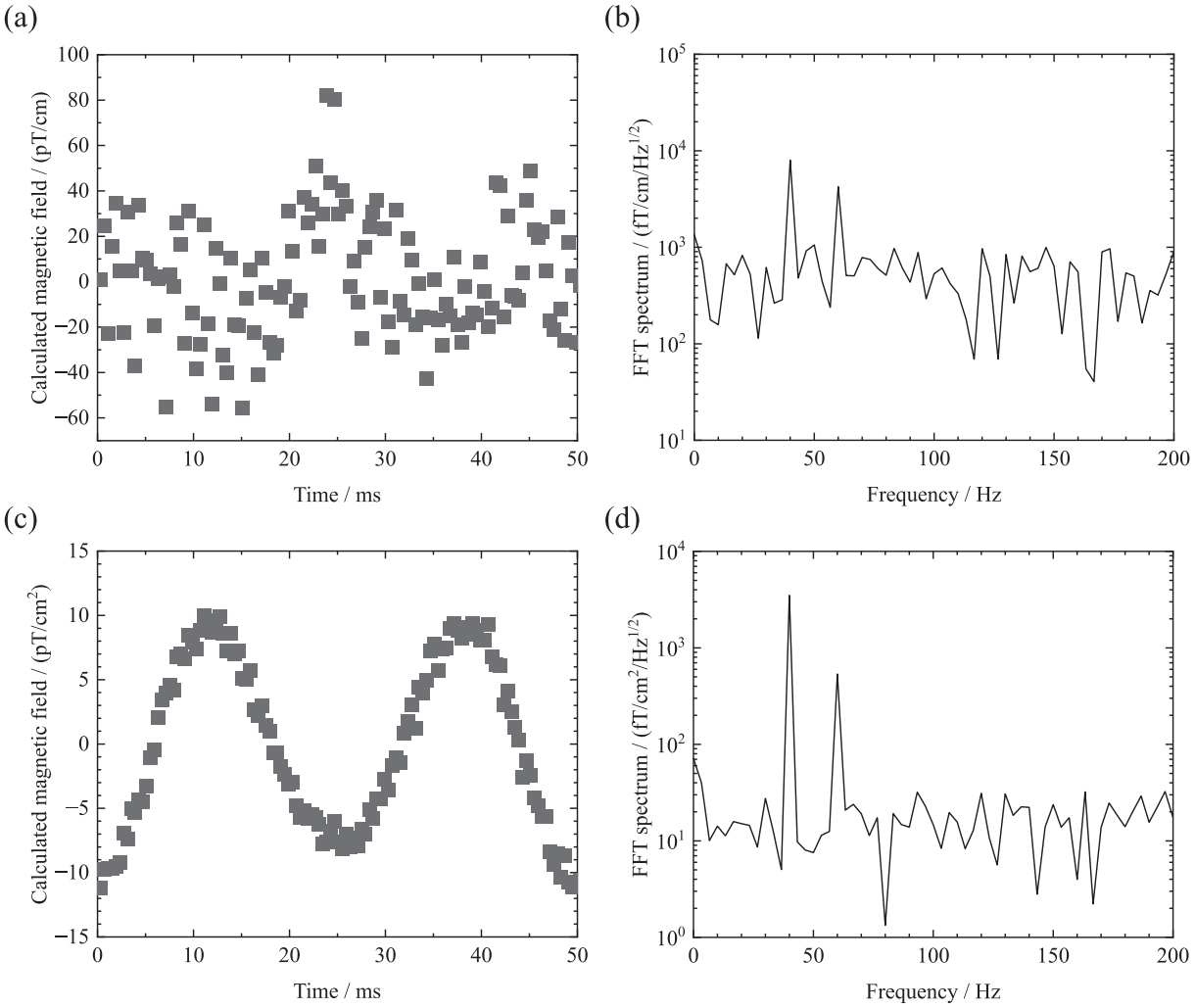

Fig. 5 (a) 1st-order differential output of obtained magnetic fields between Ch. 1 and Ch. 2, (b) Frequency spectrum of (a), (c) 2nd-order differential output of obtained magnetic fields among Ch. 1, Ch. 2, and Ch. 3, and (d) Frequency spectrum of (c).

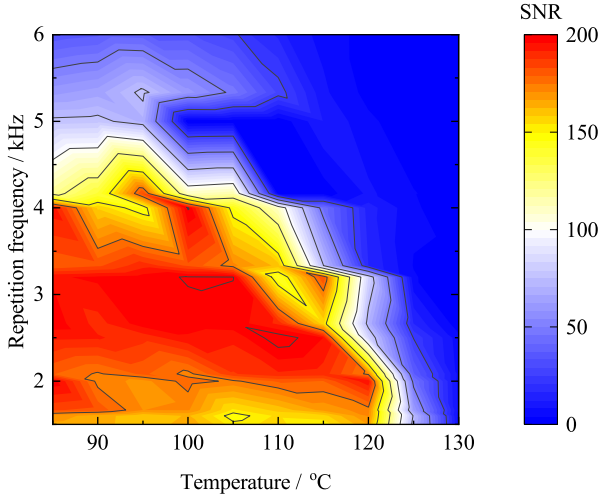

Fig. 6 Change in SNR of the 2nd-order differential output as functions of temperature and repetition frequency.

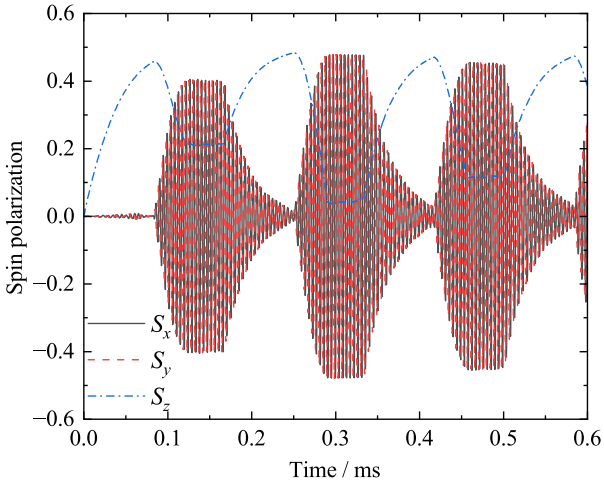

Fig. 7 Time evolution of spin polarization. Repetition frequency is 6 kHz, and temperature is 110 °C.

for each repetition. When calculating the magnetic field for each FID section using Eq. (1), we assumed the slow-down factor was used as a constant, because it is unknown in the practical measurements. However, it depends on the magnitude of the spin polarization according to Eq. (3). Thus, it was thought that an error was generated at each repetition and the magnetic field signal was not calculated properly. Therefore, when operating the scalar-mode OPM, the pump pulse duration should be sufficiently large. In the case, the repetition frequency needed to be less than 4 kHz under the present conditions.

Second, we discussed that the SNR decreased as the temperature increased. This is thought to be due to the absorption of the pump beam by potassium atoms. The pump beam attenuates as it propagates in z direction due to absorption by the potassium atoms. As a result, the pumping rate also has a spatial distribution and is given as follows [13]:

$$\frac{dR_{\mathrm{OP}}(z)}{dz} = -n_{\mathrm{K}}\sigma R_{\mathrm{OP}}(z)\{1 - 2S_z(z)\}, \tag{7}$$

where n_{K} is density of K, σ is absorption cross section of K, and S_z is the z component of the spin polarization. According to Eq. (4), the higher the temperature is, the higher K density is. It leads to the greater the attenuation of the pumping rate. Therefore, when the temperature was high, each channel had a different magnitude of the spin polarization due to the difference in pumping rate, and the slow-down factor became different in each channel according to Eq. (3). Therefore, there was an error in the calculation of the magnetic field for each channel, and the SNR was not improved even if we used differential configuration. Accordingly, when operating scalar-mode OPMs with differential configuration, we must not set the temperature too high. Under the present condition, the temperature should be less than 120 °C.

5. Conclusion

Numerical calculations show that scalar-mode OPMs with differential configuration can be used to measure very weak magnetic fields in the Earth's field. Under the ambient magnetic field in the laboratory, the noise levels were found to be 529 fT/cm/$\sqrt{\mathrm{Hz}}$ and 17.2 fT/cm^2/$\sqrt{\mathrm{Hz}}$ using the first-order and the second-order differential configurations, respectively. Also, the SNR was found to be dependent on the repetition frequency and temperature. In order to maintain the SNR, the repetition frequency should be set below 4 kHz and the temperature should be set below 120 °C.

Acknowledgments

The authors would like to thank T. Kobayashi, Kyoto University for discussion. This work was supported by a Grant-in-Aid for Research (21H03807) from the Ministry of Education, Culture, Sports, Science, and Technology (MEXT), Japan.

References

[1] D. Drung, C. Abmann, J. Beyer, A. Kirste, M. Peters, F. Ruede, and T. Schurig, "Highly Sensitive and Easy-to-Use SQUID Sensors," IEEE Trans. Appl. Supercond., vol.17, no.2, pp.699–704, 2007.
[2] J.C. Allred, R.N. Lyman, T.W. Kornack, and M.V. Romalis, "High-sensitivity atomic magnetometer unaffected by spin-exchange relaxation," Phys. Rev. Lett., vol.89, no.13, 130801, 2002.
[3] I.K. Kominis, T.W. Kornack, J.C. Allred, and M.V. Romalis, "A subfemtotesla multichannel atomic magnetometer," Nature, vol.422, no.6932, pp.596–599, 2003.
[4] M.E. Limes, E.L. Foley, T.W. Kornack, S. Caliga, S. McBride, A. Braun, W. Lee, V.G. Lucivero, and M.V. Romalis, "Portable Magnetometry for Detection of Biomagnetism in Ambient Environments," Phys. Rev. Applied, vol.14, no.1, 11002, 2020.
[5] R. Zhang, R. Mhaskar, K. Smith, and M. Prouty, "Portable intrinsic gradiometer for ultra-sensitive detection of magnetic gradient in unshielded environment," Appl. Phys. Lett., vol.116, no.14, 143501, 2020.
[6] D. Sheng, S. Li, N. Dural, and M.V. Romalis, "Subfemtotesla Scalar Atomic Magnetometry Using Multipass Cells," Phys. Rev. Lett., vol.110, no.16, 160802, 2013.
[7] S.J. Seltzer and M.V. Romalis, "Unshielded three-axis vector operation of a spin-exchange-relaxation-free atomic magnetometer," Appl. Phys. Lett., vol.85, no.20, pp.4804–4806, 2004.
[8] S. Appelt, A.B.-A. Baranga, C.J. Erickson, M.V. Romalis, A.R. Young, and W. Happer, "Theory of spin-exchange optical pumping of ^{3}He and ^{129}Xe," Phys. Rev. A, vol.58, no.2, pp.1412–1439, 1998.
[9] Y. Ito, H. Ohnishi, K. Kamada, and T. Kobayashi, "Rate-equation approach to optimal density ratio of k-rb hybrid cells for optically pumped atomic magnetometers," 2013 35th Annual International Conference of the IEEE Engineering in Medicine and Biology Society (EMBC), pp.3254–3257, July 2013.
[10] S. Ito, Y. Ito, and T. Kobayashi, "Temperature characteristics of k-rb hybrid optically pumped magnetometers with different density ratios," Opt. Express, vol.27, no.6, pp.8037–8047, March 2019.
[11] N. Allard and J. Kielkopf, "The effect of neutral nonresonant collisions on atomic spectral lines," Rev. Mod. Phys., vol.54, no.4, pp.1103–1182, 1982.
[12] K. Kim, S. Begus, H. Xia, S.-K. Lee, V. Jazbinsek, Z. Trontelj, and M.V. Romalis, "Multi-channel atomic magnetometer for magnetoencephalography: A configuration study," NeuroImage, vol.89, pp.143–151, 2014.
[13] K. Kamada, S. Taue, and T. Kobayashi, "Optimization of Bandwidth and Signal Responses of Optically Pumped Atomic Magnetometers for Biomagnetic Applications," Jpn. J. Appl. Phys., vol.50, no.5R, 56602, 2011.

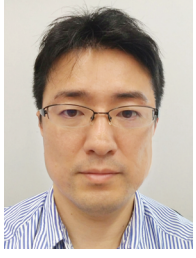

Yosuke Ito received the B. Eng., M. Eng., and Dr. Eng. degrees from Kyoto University in 2005, 2007, and 2010, respectively. He is an Junior Associate Professor in the Gradiate School of Engineering, Kyoto University. He has been engaged in biomagnetic field measurements and the development of high-sensitivity magnetometers.

Tatsuya Goto received the B. Eng. and M. Eng. degrees from Kyoto University in 2020 and 2022, respectively. During the master course in Kyoto University, he engaged in the development of scalar-mode optically pumped magnetometers.

Takuma Hori received the B. Eng. and M. Eng. degrees from Kyoto University in 2021 and 2023, respectively. During the master course in Kyoto University, he engaged in the development of scalar-mode optically pumped magnetometers.